SAND2016-4264J

Pattern Effects of Soil on Photovoltaic Surfaces

Patrick D. Burton, Alex Hendrickson, Stephen Seth Ulibarri,
Daniel Riley, William E. Boyson, Bruce H. King, *Member, IEEE*

***Abstract*—The texture or patterning of soil on PV surfaces may influence light capture at various angles of incidence (AOI). Accumulated soil can be considered a micro-shading element, which changes with respect to AOI. Laboratory deposition of simulated soil was used to prepare test coupons for simultaneous AOI and soiling loss experiments. A mixed solvent deposition technique was used to consistently deposit patterned test soils onto glass slides. Transmission decreased as soil loading and AOI increased. Dense aggregates significantly decreased transmission. However; highly dispersed particles are less prone to secondary scattering, improving overall light collection. In order to test AOI losses on relevant systems, uniform simulated soil coatings were applied to split reference cells to further examine this effect. The measured optical transmission and area coverage correlated closely to the observed I_{SC}. Angular losses were significant at angles as low as 25°.**

***Index Terms*—Soiling, surface contamination, performance loss, standardized test methods**

I. Introduction

The accumulation of soil on photovoltaic modules causes a loss in short circuit current due to the reduction in incident light. In order to offset the loss, any mitigation strategy must be resource-effective. Regular washing can be expensive in arid regions [1], so many systems are allowed to soil until naturally cleaned by rain [2]. Unfortunately, light rain or dew can often compound the problem by redispersing and concentrating dust [3]. In addition to the loss in short circuit current, non-uniform soil coverage or irregular shading can cause hot spots [4]–[6].

As the angle of incidence changes throughout the day, a non-uniform soil coating will present a changing optical profile to the underlying device. Soil particles at the module surface can be thought of as obstacles shadowing the cell. Densely stacked particles could have a greater impact on the underlying cell at high angle of incidence (AOI) than under direct irradiance.

In order to quantify losses due to irregular soil accumulation, systematic indoor and outdoor studies were conducted. By controlling particle deposition on glass surfaces, uniform or dispersed soil films were used to simulate a range of soil patterns. These patterns were used to examine the effects of extent of soil coverage and area profile on light transmission through the soiled region. The present work is an expansion to results presented at the 42nd PVSC [7] to include a study using soiled reference cells. Soil was applied to a split reference cell using an aerosol spray gun, and then cleaned off of one half of the cell. This coplanar test system was subsequently tracked through 90° in order to directly compare the reduction in current between the clean and soiled cells.

This work was supported by the U.S. Department of Energy SunShot Initiative. Sandia National Laboratories is a multi-program laboratory managed and operated by Sandia Corporation, a wholly owned subsidiary of Lockheed Martin Corporation, for the U.S. Department of Energy's National Nuclear Security Administration under contract DE-AC04-94AL85000.

P. D. Burton (e-mail: pdburto@sandia.gov), S. S. Ulibarri, D. Riley, W. E. Boyson and B. H. King are with Sandia National Laboratories, Albuquerque, NM 87185 USA.

A. Hendrickson is presently at Pennsylvania State University, State College, PA USA

Manuscript received April 27, 2016

II. Experimental Methods

Both indoor and outdoor tests were performed to examine the impact of soil patterning and AOI on the reduction in I_{SC} due to soiling. Test methods are described in this section and test results are presented in the following section.

A. Single Droplet Soil Deposition

A single droplet technique was developed to deposit dense soil coatings on small regions of the test coupon. Test soil was suspended in an organic solvent and cast from a mounted microliter pipettor onto the test coupon. As the droplet dried, the suspended soil was deposited in place. Fast and slow drying solvents [acetonitrile (ACN, Reagent Grade, Sigma Aldrich), and ethanol (EtOH, 200 proof, Sigma Aldrich), respectively] were mixed to provide a controlled range of drying times.

Glass slides (Petrographic microscope slides, Ward's Science) were rinsed in DI H_2O, followed by EtOH. Each slide was placed in a machined slide holder held in position under a 10 µl pipetteor. A commercial test dust (AZ road dust, Powder Technology Incorporated, ISO 12103-1 A2 Fine) was suspended in a mixed carrier solvent. Ratios of ACN and EtOH [0, 20, 40, 60, 80 and 100 % ACN:EtOH] were used as carrier solvents. A single soil composition was used to focus on geometric patterning, not compositional uniformity. Suspension concentrations of 0.01 or 0.02 g/ml were deposited by ejecting a single drop onto the glass surface and allowing it to dry. The soil applied in this manner was below the detectable limit of the mass balance. Samples were quantified by measurement of the dried droplet area only. Results are quantified in terms of the area obscured by the soil in square centimeters. The various solvents used dried at different rates, producing a range of dried dust spots on each coupon.

For each technique, the area coverage of the applied sand was determined at macroscopic and microscopic length scales using a Canon 10D digital camera and Olympus IX71 microscope equipped with a DP72 camera, respectively. Each image was imported into ImageJ [8] for automated particle analysis. Most single droplets were sufficiently contiguous to measure the entire region using a pixel counting program. For samples with irregular areas, the region of interest (ROI) was outlined by hand and measured. Each area was measured in triplicate.

B. Angle of Incidence

UV/vis/NIR spectroscopic measurements were collected with a Varian Cary 5000 UV/vis/NIR spectrophotometer. Angle of incidence effects were evaluated by placing the test slide in a variable angle sample holder in a DRA-2500 diffuse reflectance accessory. Scans were collected at 10° intervals. Baseline measurements were collected with a clean reference sample mounted in the holder at 0°. This differs from the procedure described by [10], who use an empty chamber for the reference condition. This configuration was chosen in order to reference all measurements to a perpendicular incident beam. The reference condition thus mimics normal incident geometry. Transmittance was calculated for spot-soiled samples by collecting one scan with a Specralon® reference at the exit port, capturing both transmittance and reflectance data simultaneously, as described in eq. (1). The sample reflectance port was subsequently replaced with a light trap, ensuring that only the scattered light was collected (eq. (2)). Transmittance was calculated using the coupled equations shown in eq. (3).

$$A_1 = -\log(T + R) \tag{1}$$

$$A_2 = -\log(R) \tag{2}$$

$$T = \exp(-A_1) - \exp(-A_2) \tag{3}$$

C. Reference Module Preparation

A spray technique was used to apply a synthetic soil (3% soot, 97% AZ dust, see [9]) suspended in ACN to assembled split reference cells. This mixture differs from the single spot tests described above and was selected to more accurately match outdoor conditions. Split single crystal Si cells (PV Measurements, Inc.) were used to compare the change in irradiance due to deposited soil. The module cover glass was AGC Solite with a diamond patterned surface. Each half-cell was shunted, allowing a comparison to be made between each side (clean and soiled) of the device. The entire framed module was soiled, then half of the face was cleaned to expose one half-cell. Clean, dry witness coupons were placed at the corners to minimize cell overlap as much as possible (Fig. 1). The aerosol gun was held above the flat-mounted cell to ensure that the plume fully encompassed the area. The mass of each coupon was determined before and after soiling, and the average was used as the module soiling level. After the coupons were removed, half of the module was wiped clean and used as a coplanar reference.

D. Outdoor AOI Test

Prepared split-cell reference modules (see Fig. 1) were mounted on a two-axis tracker and tracked through 90° in elevation only, as described in [11]. The measured loss $(f_2(\theta))$ was calculated using eq. (4).

$$f_2(\theta) = \frac{\left[\frac{I_{SC}}{I_{SCr}}\right]\left[\frac{E_0}{1+\alpha_{ISC}(T_C - T_0)}\right] - E_{Diff}}{E_{DNI}\cos\theta} \tag{4}$$

In the preceding equation, I_{SCr} is the reference short circuit current, E_0 is the reference irradiance, α_{ISC} is the short circuit temperature coefficient, E_{Diff} is the global diffuse irradiance, and E_{DNI} is the direct normal irradiance. See [11] for a full derivation. During the experiment, E_{Diff} was collected using a Kipp & Zonen CMP22 pyranometer mounted in the module test plane with a shade band. A Kipp & Zonen CHP1 pyrheliometer mounted independently of the tracker was used to measure E_{DNI}. The I_{SC} and T_C for each channel of the reference cell were measured continuously using an Agilent 34970A data logger and Labview software.

The percent soiling loss at 0° for each module was found by comparing the ratio of I_{SC} for the soiled and cleaned cells. Angular responses were evaluated using $(f_2(\theta))$.

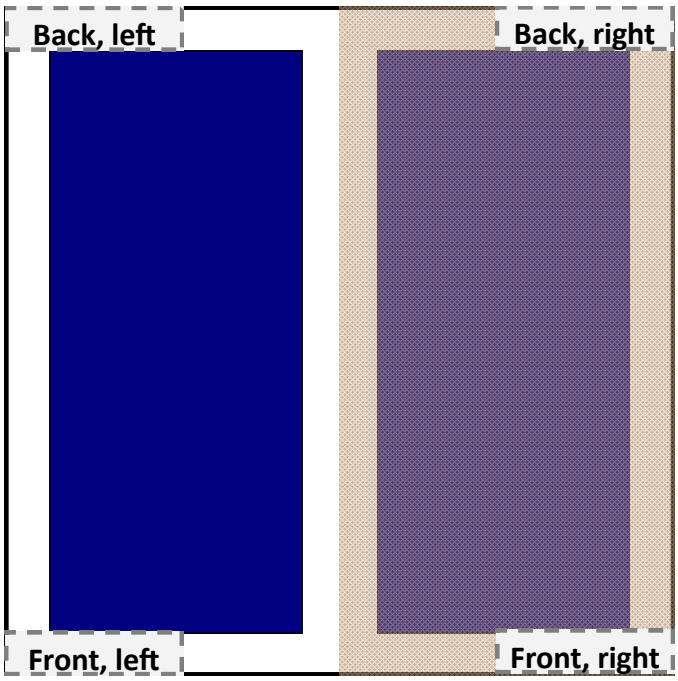

Fig. 1. Schematic of split reference cell with witness coupon positions front left (FL), front right (FR), back left (BL) and back right (BR).

III. Results and Discussion

A. Spot Soiling

In order to address uniformity and AOI effects in a consistent manner, small soil droplets were deposited on glass slides at varying deposition densities. Solvent ratios were varied (section II-A) to control the density and patterning of the dried droplet. The applied mass was below the gravimetric detection limit, so soil loadings have been reported in terms of the total area of the dried soil film. Each sample prepared using ACN as a carrier solvent exhibited some degree of pattern formation (Figs. 2a to 2e), while the 0% ACN (100% EtOH) samples were homogeneous, as well as less dense (Fig. 2f) due to a greater total area coverage. The lower volatility solvent spread over a larger area before it evaporated, allowing the suspended particulates to settle slowly. In contrast, the high volatility ACN evaporated quickly, producing patterns due to particle accumulation at the drying edge. As would be expected, the 100% ACN samples exhibited this effect to the greatest extent (Fig. 2a).

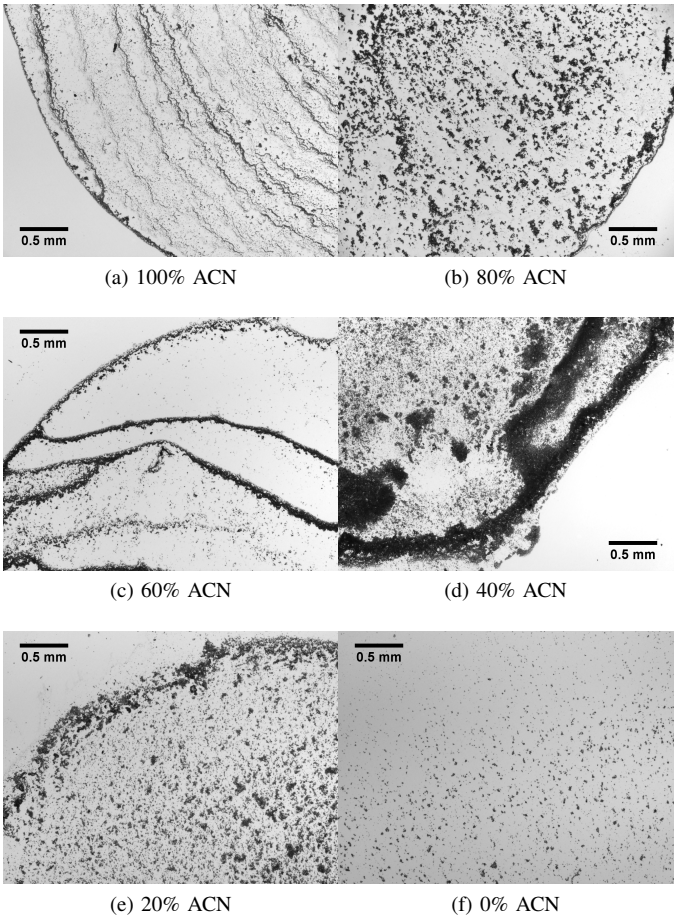

(a) 100% ACN (b) 80% ACN

(c) 60% ACN (d) 40% ACN

(e) 20% ACN (f) 0% ACN

Fig. 2. (a-f) Edges of spot soiled coupons imaged at 2.52x.

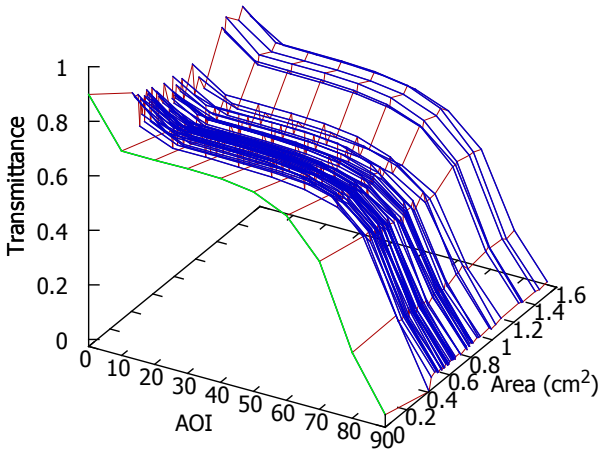

Fig. 3. Surface plot of transmittance with respect to AOI and area coverage for spot-soiled samples. The clean reference is shown in green at 0 cm^2. All samples prepared using ACN grouped between 0.4 and 0.6 cm^2. The 0% ACN samples correlate to 1.4 to 1.6 cm^2. A two dimensional projection of Transmittance with respect to Area is shown in Fig. 4.

The magnitude of the measured transmittance was similar for the entire range of samples. The trend of each AOI response likewise remained consistent from 10 to 50°. Due to the instrument geometry, specular reflectance at 0° was lost through the beam port of the integrating sphere, but was collected at all other sample positions. As a result, a discontinuity was noted between 0 and 10° (see Fig. 3).

The specular reflectance loss (and by extension, the reduction in transmission) was comparable for all samples except those prepared using 0% ACN as the dispersion solvent, as shown in Figs. 3 and 4. The response decreased slowly in the range from 10-50°. The fractional change in illuminated area was small, so most spot types intercepted a similar percentage of the incident light. The 0% ACN samples were the exception, which are noticeably offset from the majority of the traces in Fig. 3. This trend can be more clearly seen by the abrupt change within the highlighted region in Fig. 4. The overall trend held until 80°, at which point the transmittance was nearly identical for all samples. In this geometry, the edge of the soil spot is exposed to the beam, shading the remaining area. Patterning is relatively insignificant in this scenario, as very little of the soiled face is exposed to the beam.

The transmittance of the spot-soiled coupons can be used to illustrate an intuitive, but significant issue in soil accumulation. For a given amount of soil, losses are minimized when the particulates (or aggregates) are as dispersed as possible. No single trend could be determined among the patterned samples, except that they all exhibited a greater decrease in transmission than the 0% ACN samples with a uniform particle coverage. Particles distributed over a greater area are less prone to secondary scattering, improving overall light collection.

B. Outdoor

Split reference cells were spray-coated with grime suspended in ACN and placed outdoors for AOI tests. The witness coupons for each module were analyzed to determine soil loading, area coverage and light transmission. The decrease in transmission was proportional to the increase in area coverage (Fig. 5). Soil patterning was evaluated on the basis of the measured area coverage determined by witness coupons. As the soil loading increases, the pattern of the deposits becomes more irregular, as seen in the trend in Fig. 5. Very low mass loadings (note points below 1 g/m^2) exhibit a much smaller standard deviation than heavy loadings (esp. 3 g/m^2 and greater). In addition to the greater amount of soil present on these coupons, the dispersion of the soil is more irregular.

The average of each set of witness coupons was used as the soil loading for the entire reference module. The left side of each split cell (see Fig. 1) was cleaned with a dry cloth prior to mounting on a 2-axis tracker. The I_{SC} was simultaneously measured for both clean and soiled subcells as the tracker was positioned through a range of incident angles. For comparison to the measured (UV/vis) transmission loss and obscured area, the ratio of raw I_{SC} at 0° for the clean and soiled sides of each reference cell was calculated (Fig. 5).

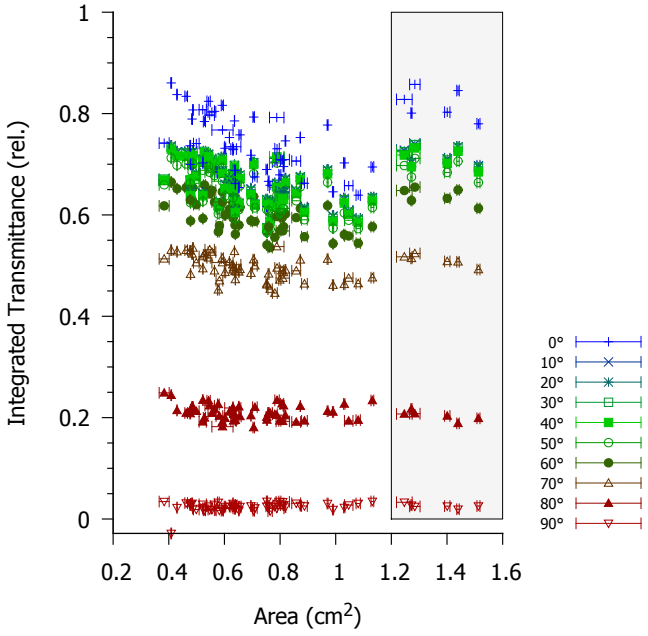

Fig. 4. AOI response of spot-soiled coupons. An overall decreasing trend is observed at 0-50° up to an area coverage of ∼1.1 cm^2. Area coverage greater than this value (produced by 0% ACN dispersion) corresponds to an abrupt increase in the integrated transmittance. These points are highlighted within the shaded region.

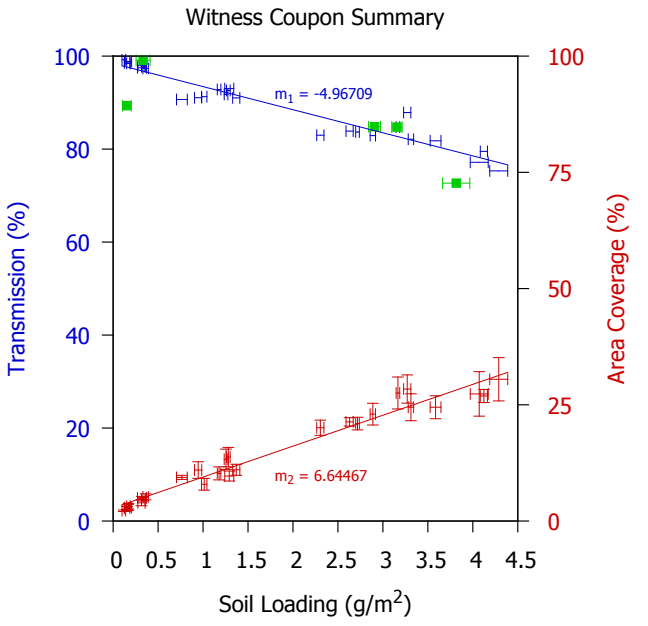

Fig. 5. The transparency of witness coupons is inversely correlated to the measured area coverage. Solid points correspond to the ratio of I_{SC} for the reference cells expressed as a percentage.

Angular losses $[f_2(\theta)]$ due to soiling were calculated using eq. (4) and are immediate for all angles $> 0°$. The effect becomes more apparent when the ratio of the clean and soiled channels is examined, as in Fig. 6. A control experiment was conducted using a completely clean reference device.

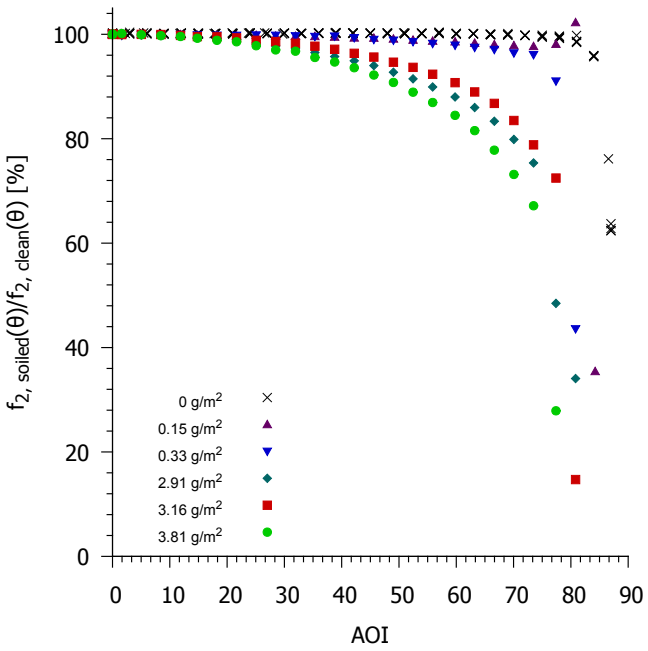

Fig. 6. The ratio $f_{2,soiled}(\theta)/f_{2,clean}(\theta)$ shows a clear trend between minimum and maximum soil loading.

The ratio of the two half-cells was constant, as expected, until ∼50°. Since both cells are clean, this change in relative output is entirely geometrical. The normalized loss $[f_{2,soiled}(\theta)/f_{2,clean}(\theta)]$ was approximately proportional to mass loading. The extent of this loss correlates to the order of magnitude of the applied soil. This is indicative of an increase in reflectance, as has been discussed previously [11], [12]. For practical purposes, the ratio of $f_{2,soiled}(\theta)/f_{2,clean}(\theta)$ is an indicator of the extent of soiling. The angular loss ratio is nearly flat for minimally soiled (Fig. 7a) cells, until geometric limitations above ∼80°.

It was observed that soiling had an immediate impact on the angle of incidence response of the test coupons, causing losses in short circuit current under off-axis conditions that were greater than would be expected based on either direct normal or transmission measurements. For light soil loading (∼ 0.25 g/m^2), the deviation was on the order of a few percent up to an AOI of around 40-50°, after which the deviation increased to ∼10%. However, at higher mass loadings (> 2.5 g/m^2), the effect became much more pronounced. Interestingly, the $f_2(\theta)$ response for the 2.91 g/m^2 sample was lower than the next larger sample, 3.16 g/m^2. At 0°, the transmission through both samples is very similar (see solid points in Fig. 5); however, small variations in soil texture likely resulted in a more pronounced AOI response.

Significant deviation was observed at small AOI, around 10-20° and the deviation was up to ∼20% at 50°. As the extent of soiling increased, the normalized losses became evident at progressively smaller AOI. For extreme cases of soiling, dense aggregates would be expected to have the greatest potential to cast large shadows at high AOI.

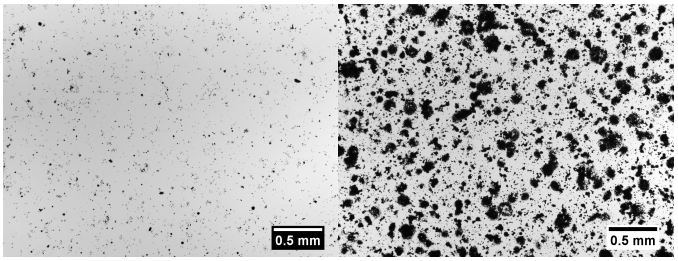

(a) 0.15 g/m^2 (b) 3.81 g/m^2

Fig. 7. Witness coupons at 0.15 g/m^2 (a) and 3.81 g/m^2 loading (b) imaged at 2.52x.

IV. Conclusion

The amount of accumulated soil and the dispersion over the surface are critical aspects to PV soiling losses. Highly uniform soiling (i.e. discrete particulates with few to no aggregates, such as the 0% ACN sample in Fig. 2f) was more transparent than a similar soil loading in irregular patterns. The implications of these observations are significant, particularly in the case of commercial, rooftop PV systems. Such systems are typically deployed at shallow angles of 10°. At these shallow angles, the sun will only be directly overhead for systems installed at low latitudes and then only at the summer solstice. For all other installations, the system will always be at a non-optimal high incident angle configuration. Further, we have previously observed that soil accumulation is much more rapid at shallow tilt angles than at the higher tilt angles that are more common for ground mount utility systems. Exacerbated by sporadic (or nonexistent) cleaning schedules, these systems may thus be doubly susceptible to losses due to soil accumulation. Preventing dense soil deposits, rather than the absolute cleanliness of the module, may be an effective soil mitigation strategy.

Acknowledgment

The authors thank Matthew Lave for helpful discussions. This work was supported by the U.S. Department of Energy SunShot Initiative. Sandia National Laboratories is a multi-program laboratory managed and operated by Sandia Corporation, a wholly owned subsidiary of Lockheed Martin Corporation, for the U.S. Department of Energy's National Nuclear Security Administration under contract DE-AC04-94AL85000.

References

[1] L. L. Kazmerski, M. Al Jardan, Y. Al Jnoobi, Y. Al Shaya, and J. J. John, "Ashes to ashes, dust to dust: Averting a potential showstopper for solar photovoltaics," in *Photovoltaic Specialist Conference (PVSC), 2014 IEEE 40th*, 2014, pp. 0187–0192.

[2] A. Kimber, L. Mitchell, S. Nogradi, and H. Wenger, "The Effect of Soiling on Large Grid-Connected Photovoltaic Systems in California and the Southwest Region of the United States," in *Photovoltaic Energy Conversion, Conference Record of the 2006 IEEE 4th World Conference on*, vol. 2, 2006, pp. 2391–2395.

[3] T. Sarver, A. Al-Qaraghuli, and L. L. Kazmerski, "A comprehensive review of the impact of dust on the use of solar energy: History, investigations, results, literature, and mitigation approaches," *Renewable and Sustainable Energy Reviews*, vol. 22, no. 0, pp. 698–733, 2013.

[4] E. Lorenzo, R. Moretón, and I. Luque, "Dust effects on PV array performance: in-field observations with non-uniform patterns," *Progress in Photovoltaics: Research and Applications*, pp. n/a–n/a, 2013.

[5] E. E. van Dyk, E. L. Meyer, F. J. Vorster, and A. W. R. Leitch, "Long-term monitoring of photovoltaic devices," *Renewable Energy*, vol. 25, no. 2, pp. 183–197, 2002.

[6] M. Drif, P. J. Pérez, J. Aguilera, and J. D. Aguilar, "A new estimation method of irradiance on a partially shaded pv generator in grid-connected photovoltaic systems," *Renewable Energy*, vol. 33, no. 9, pp. 2048–2056, 2008.

[7] P. D. Burton, A. Hendrickson, and B. H. King, "Macro- and Microscale Particle Size Effects of Soil on Photovoltaic Surfaces," in *Photovoltaic Specialist Conference (PVSC), 2015 IEEE 42nd*, 2015, pp. 1–5.

[8] W. S. Rasband, "ImageJ," 1997-2012. [Online]. Available: http://imagej.nih.gov/ij/

[9] P. D. Burton and B. H. King, "Application and Characterization of an Artificial Grime for Photovoltaic Soiling Studies," *Photovoltaics, IEEE Journal of*, vol. 4, no. 1, pp. 299–303, 2014.

[10] S. L. Storm, A. Springsteen, and T. M. Ricker, "The use of center mount sample holders in reflectance spectroscopy," 1998.

[11] B. H. King, D. Riley, C. R. Robinson, and L. Pratt, "Recent Advancements in Outdoor Measurement Techniques for Angle of Incidence Effects," in *Photovoltaic Specialists Conference, 2015. Conference Record of the Forty Second IEEE*, 2015, pp. 1–6.

[12] N. Martin and J. M. Ruiz, "Calculation of the PV modules angular losses under field conditions by means of an analytical model," *Solar Energy Materials and Solar Cells*, vol. 70, no. 1, pp. 25–38, 2001.